RESEARCH LETTER

Key Points:
- Analyzed scaling of precipitation extremes in radiative-convective equilibrium
- Representation of ice- and mixed-phase microphysics plays an important role
- Response to warming depends on accumulation period at low temperatures

Correspondence to:
M. S. Singh,
mssingh@MIT.EDU

Influence of microphysics on the scaling of precipitation extremes with temperature

Martin S. Singh[1] and Paul A. O'Gorman[1]

[1]Department of Earth, Atmospheric and Planetary Sciences, Massachusetts Institute of Technology, Cambridge, Massachusetts, USA

Abstract Simulations of radiative-convective equilibrium with a cloud-system resolving model are used to investigate the scaling of high percentiles of the precipitation distribution (precipitation extremes) over a wide range of surface temperatures. At surface temperatures above roughly 295 K, precipitation extremes increase with warming in proportion to the increase in surface moisture, following what is termed Clausius-Clapeyron (CC) scaling. At lower temperatures, the rate of increase of precipitation extremes depends on the choice of cloud and precipitation microphysics scheme and the accumulation period, and it differs markedly from CC scaling in some cases. Precipitation extremes are found to be sensitive to the fall speeds of hydrometeors, and this partly explains the different scaling results obtained with different microphysics schemes. The results suggest that microphysics play an important role in determining the response of convective precipitation extremes to warming, particularly when ice- and mixed-phase processes are important.

1. Introduction

Increases in the intensity of precipitation extremes are seen in simulations of global warming [*Kharin et al.*, 2007; *O'Gorman and Schneider*, 2009] and have been identified in observational trends [*Westra et al.*, 2013]. However, the rate at which precipitation extremes will strengthen as the climate warms remains uncertain to the extent that they involve moist-convective processes that are difficult to represent in climate models [*Wilcox and Donner*, 2007; *O'Gorman*, 2012; *Kendon et al.*, 2014]. Observations of variability in the current climate may also be used to derive relationships between precipitation extremes and the temperature at which they occur [e.g., *Allan et al.*, 2010], and analyses based on station observations have found that the fractional increase in subdaily precipitation extremes with respect to temperature is up to twice that of daily precipitation extremes [*Lenderink and van Meijgaard*, 2008; *Lenderink et al.*, 2011; *Berg et al.*, 2013]. However, this dependence on timescale is not well understood, and it is unclear whether such relationships would also hold under global warming.

Here we investigate the precipitation distribution in simulations with a cloud-system resolving model in the idealized setting of radiative-convective equilibrium (RCE). Previous studies of the precipitation distribution in RCE have found that, at surface temperatures characteristic of Earth's tropics, precipitation extremes increase with warming following what is known as Clausius-Clapeyron (CC) scaling, increasing roughly in proportion to the saturation specific humidity near the surface [*Muller et al.*, 2011; *Romps*, 2011]. This conclusion holds even when the convection is organized [*Muller*, 2013]. CC scaling of precipitation extremes with surface temperature is consistent with a simple view of the response of strong precipitation events to warming in which the amount of converged water vapor increases due to the increased amount of moisture near the surface. However, the close agreement with CC scaling found in studies of RCE may be coincidental to some extent because the water vapor convergence does not occur only at the surface, and because the strength and vertical profile of the updrafts change with warming [*Muller et al.*, 2011; *Romps*, 2011].

In this study, we extend previous modeling results to a wider range of surface temperatures. Consistent with previous work, precipitation extremes increase with warming at a rate similar to that implied by CC scaling at surface temperatures above 295 K. At lower temperatures, however, the scaling of precipitation extremes depends on the representation of cloud and precipitation microphysics used in the simulations as well as the accumulation period considered. Instantaneous precipitation extremes increase with warming at up to twice the rate implied by CC scaling for one of the microphysics schemes used.

One factor contributing to such high rates of increase is a change in the mean fall speed of hydrometeors in a warming atmosphere. The precipitation distribution is known to be sensitive to hydrometeor fall speed [*Parodi and Emanuel*, 2009; *Parodi et al.*, 2011]; here we find that as the atmosphere warms, the fraction of the precipitating water in the column composed of frozen hydrometeors decreases, and the mean fall speed of hydrometeors increases, amplifying the increase in precipitation extremes. But the degree to which the fall speed increases with warming is sensitive to assumptions regarding the treatment of frozen hydrometeors, and hydrometeor fall speed is not the only microphysical property to have an influence on precipitation extremes. As a result, different microphysics schemes lead to different scaling of precipitation extremes with warming at surface temperatures for which ice- and mixed-phase microphysical processes are important, even in the relatively simple case of RCE.

2. Simulations of Radiative-Convective Equilibrium

We analyze simulations of RCE in a doubly periodic domain conducted using version 16 of the Bryan Cloud Model [*Bryan and Fritsch*, 2002]. *Singh and O'Gorman* [2013] used a similar set of simulations to investigate increases in convective available potential energy with warming. The model is compressible and nonhydrostatic, and it uses sixth-order spatial differencing coupled with a sixth-order diffusion scheme for numerical stability and a split-explicit time-stepping scheme following *Wicker and Skamarock* [2002]. Surface fluxes are calculated using bulk aerodynamic formulae, while subgrid motions are parameterized through a Smagorinsky turbulence scheme. Interactive radiation is included, but there is no diurnal cycle; all simulations are performed with a constant solar flux of 390 W m^{-2} incident at a zenith angle of 43°.

Our primary focus is on simulations conducted using a six-species, one-moment microphysics scheme based on *Lin et al.* [1983] as modified by *Braun and Tao* [2000] in which there are three hydrometeor species (rain, snow, and hail), each with a different fall speed that depends on the mixing ratio. We refer to this as the Lin-hail scheme. Additionally, we consider simulations with an alternate form of the *Lin et al.* [1983] scheme in which the hail category is replaced by a graupel category, which we refer to as the Lin-graupel scheme. The major difference between these two schemes is that the density, mean size, and fall speed of hail are taken to be considerably larger than those of graupel. Finally, we consider simulations conducted using a third microphysics scheme based on that of *Thompson et al.* [2008]. This scheme also includes six water species, but it additionally includes prognostic variables representing the number concentration of cloud ice and (in the implementation used here) rain water, effectively being a two-moment scheme for these species. Further details of the microphysics schemes used in this study are given in section S1 in the supporting information.

Simulations are conducted with different imposed CO_2 concentrations in the range 1–640 ppmv and at three different horizontal resolutions. First, a set of low-resolution simulations (2 km horizontal grid spacing, 80 × 80 km domain) are run to equilibrium over a slab ocean using the Lin-hail microphysics scheme. The slab has a depth of 1 m and a horizontally uniform temperature that responds to domain-integrated energy fluxes at the surface. The wide range of CO_2 concentrations used allows the slab ocean simulations to achieve equilibrium sea surface temperatures (SSTs) in the range 281–311 K. While the varying CO_2 concentration also affects radiative cooling rates in the simulations, previous work suggests that changes in the magnitude of tropospheric radiative cooling may have only a weak effect on precipitation intensity in RCE [see Figure 3 of *Parodi and Emanuel*, 2009]. Nevertheless, the low CO_2 concentration used in the coldest simulations and the lack of large-scale forcing in RCE must be taken into account when comparing our results to observations of convective precipitation extremes at similar surface temperatures on Earth.

A set of intermediate-resolution simulations (1 km horizontal grid spacing, 84 × 84 km domain) and a set of high-resolution simulations (0.5 km horizontal grid spacing, 160 × 160 km domain) are then conducted using the Lin-hail scheme over the same range of CO_2 concentrations and using the equilibrium SSTs of the corresponding slab ocean simulations as a fixed lower boundary condition. Finally, a subset of the intermediate-resolution simulations are repeated using the alternate microphysics schemes (Lin-graupel and Thompson). All simulations include 64 vertical levels, and the intermediate-resolution (high-resolution) simulations are each run for 40 (30) days with statistics collected at hourly intervals after 20 days of simulation. While the behavior of precipitation extremes is broadly similar across resolutions, we primarily show results from the intermediate-resolution simulations in order to directly compare the different microphysics schemes. Results for the high-resolution, Lin-hail simulations are shown in Figure S1.
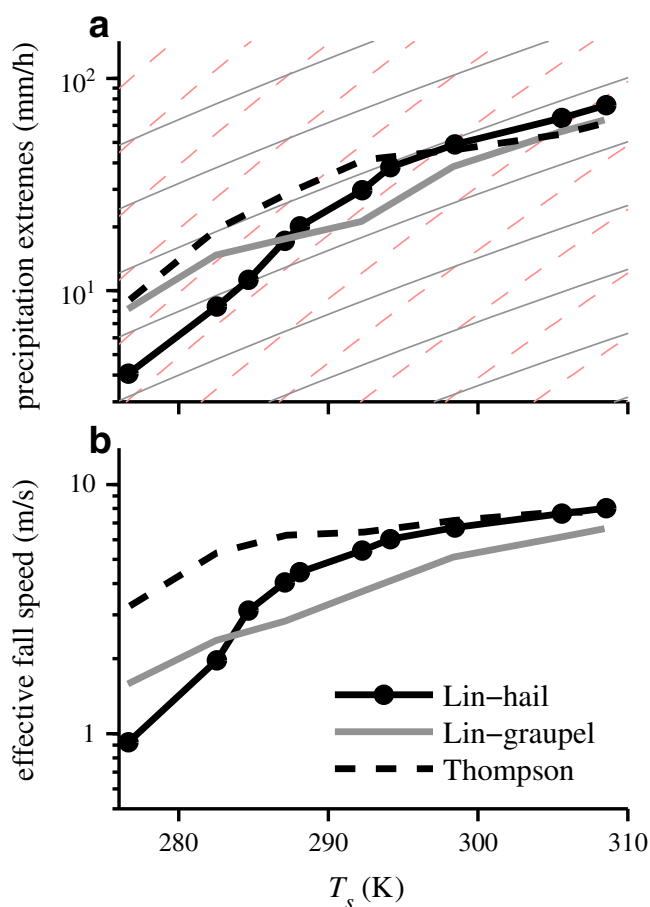
Figure 1. (a) The 99.99th percentile of the instantaneous precipitation rate and (b) the effective hydrometeor fall speed conditioned on the precipitation exceeding its 99.99th percentile (v_f). Simulations using the Lin-hail (black), Lin-graupel (thick gray), and Thompson (dashed) microphysics schemes are shown as a function of the mean temperature at the lowest model level (T_s). In Figure 1a, thin gray lines are contours proportional to the surface saturation specific humidity, and red dashed lines are proportional to the square of the surface saturation specific humidity; each successive line corresponds to a factor of 2 increase.

3. Scaling of Precipitation Extremes

Figure 1a shows precipitation extremes as measured by the 99.99th percentile of instantaneous gridbox precipitation rates as a function of the mean temperature at the lowest model level (T_s; the lowest level is at 50 m). Here instantaneous precipitation rates are measured by the flux of hydrometeors through the lower boundary at a given time step, and zero precipitation rates are included in the calculation of percentiles. The 99.99th percentile is taken to be representative of the extremes in these simulations; higher percentiles behave similarly, but lower percentiles begin to behave more like the mean precipitation intensity (the mean precipitation rate in precipitating gridboxes), and this is left for future study. For surface temperatures above 295 K, the rate of increase of precipitation extremes with warming is similar to that implied by CC scaling (gray lines) for all microphysics schemes considered, although it is slightly sub-CC in the Thompson simulations. At lower temperatures, however, the scaling of precipitation extremes is strongly dependent on the microphysics scheme used. For simulations with the Lin-hail scheme, instantaneous precipitation extremes increase rapidly with temperature, exceeding the rate of increase given by CC scaling (6–7% K^{-1}) and approaching twice that rate (red dashed lines). (Slightly higher rates of increase
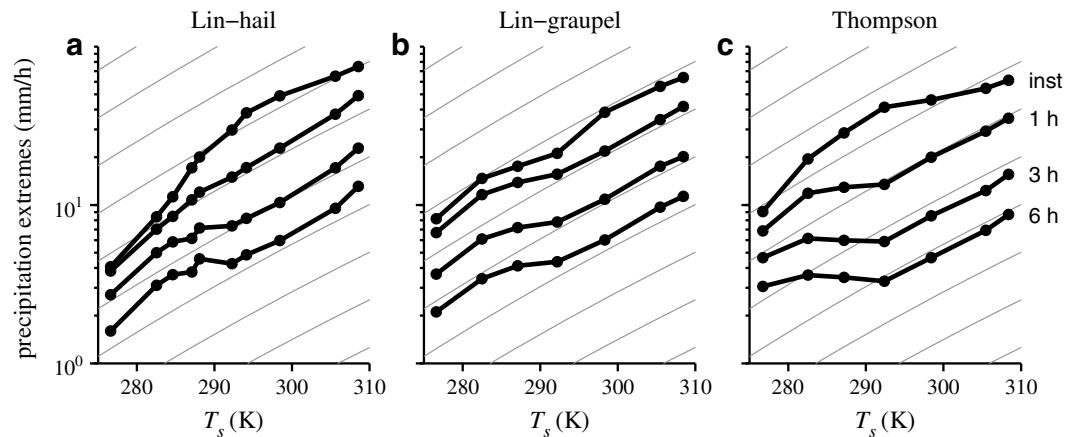
are found if the SST is used instead of T_s as a measure of the surface temperature.) Scaling of precipitation extremes above the CC rate is also found for the Thompson simulations, but only over a much narrower range of surface temperatures than for the Lin-hail simulations. For the Lin-graupel simulations, the increase in precipitation extremes with warming varies somewhat with temperature but remains relatively close to the CC rate.

Figure 2 shows precipitation extremes for 1, 3, and 6 h accumulation periods in addition to the instantaneous precipitation extremes shown earlier (daily precipitation extremes are also shown for the high-resolution, Lin-hail simulations in Figure S1). As with the instantaneous precipitation extremes, the scaling of the accumulated precipitation extremes is relatively robust at high surface temperatures, and it is similar to CC scaling for all microphysics schemes. At lower temperatures, however, the rate of increase of accumulated precipitation extremes with warming varies with temperature and the microphysics scheme used. For example, for surface temperatures below 295 K, the 6-hourly precipitation extremes increase with warming at close to the CC rate in the Lin-hail simulations, whereas in the Thompson simulations they increase weakly or decrease with warming. Both the Thompson simulations and the Lin-hail simulations (but not the Lin-graupel simulations) have much greater fractional increases in instantaneous precipitation extremes compared with 6-hourly precipitation extremes for temperatures below 295 K.

Figure 2. The 99.99th percentile of the instantaneous precipitation rate (inst) and precipitation rate averaged over 1 h, 3 h, and 6 h in simulations with (a) Lin-hail, (b) Lin-graupel, and (c) Thompson microphysics schemes (black). Gray lines are contours proportional to the surface saturation specific humidity with each successive line corresponding to a factor of 2 increase.

In the following sections we seek to understand which aspects of the different microphysics schemes lead to the differences in the scaling of precipitation extremes and the deviations from CC scaling documented above. While accumulated precipitation rates also vary across the microphysics schemes considered, we focus on instantaneous precipitation extremes because they are simpler to analyze.

4. Scaling of Condensation Extremes

We first consider extremes of the instantaneous column net-condensation rate, which we define as the vertical integral over the column of the net microphysical sink of water vapor at a given time step. In contrast to the scaling of instantaneous precipitation extremes, net-condensation extremes roughly follow CC scaling at all temperatures (Figure 3a) as well as across the three microphysics schemes (Figure S2). The roughly CC scaling of net-condensation extremes occurs despite the peak vertical velocity conditioned on net-condensation extremes increasing substantially with warming (Figure S3). As explained by *Muller et al.* [2011] and discussed in detail in section S2, the net-condensation rate is particularly sensitive to the vertical velocity at low levels. In our simulations, the vertical velocity conditioned on net-condensation extremes
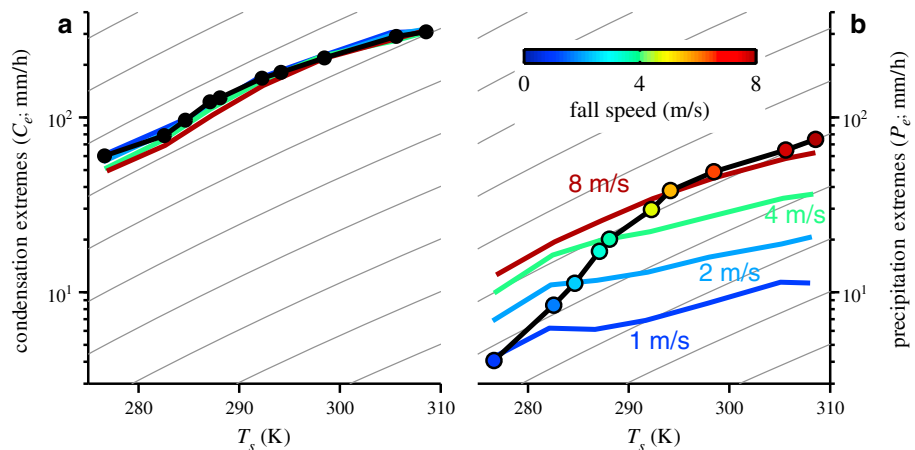

Figure 3. The 99.99th percentile of instantaneous (a) column net-condensation rate and (b) surface precipitation rate as a function of the mean temperature of the lowest model level (T_s). Black lines correspond to Lin-hail simulations and colored lines correspond to altered Lin-hail simulations in which the fall speeds of all hydrometeors are set to constant values of 1 (blue), 2 (cyan), 4 (green), and 8 (maroon) m s^{-1}. Marker colors in Figure 3b correspond to the effective fall speed (v_f) of hydrometeors in the Lin-hail simulations (see text). Thin gray lines are contours proportional to the surface saturation specific humidity, with each successive line corresponding to a factor of 2 increase.

decreases with warming at levels below 800 hPa. Consistent with *Muller et al.* [2011], low-level changes in vertical velocity, therefore, have a negative influence on net-condensation extremes, explaining how the peak updraft increases, but the net-condensation rate roughly follows CC scaling.

The simulations using the Thompson scheme experience a slightly larger increase in net-condensation extremes (Figure S2) and peak updraft strength (Figure S3) with warming compared to the Lin-hail and Lin-graupel simulations. These dynamical differences, however, are relatively small, and differences in condensation extremes are not sufficient to explain the different scaling of precipitation extremes across the different microphysics schemes used.

5. The Effect of Hydrometeor Fall Speed on Instantaneous Precipitation Extremes

It is useful to represent the relationship between instantaneous net-condensation extremes and instantaneous precipitation extremes by an efficiency ϵ_P such that

$$P_e = \epsilon_P C_e, \tag{1}$$

where P_e and C_e are the 99.99th percentiles of the instantaneous precipitation rate and instantaneous column net-condensation rate, respectively. Since we consider net condensation and since the occurrence of precipitation extremes may not be exactly collocated in space and time with the occurrence of net-condensation extremes, ϵ_P is not a conventional precipitation efficiency. Nevertheless, ϵ_P represents the efficiency by which large net-condensation events are translated into large precipitation events as the condensate falls to the surface.

The behavior of ϵ_P differs across simulations using different microphysics schemes. For simulations with the Lin-hail scheme, the fractional rate of increase of instantaneous precipitation extremes with warming is larger than that of instantaneous net-condensation extremes at low temperatures, indicating that ϵ_P increases with warming (Figure 3). For the Lin-graupel and Thompson simulations, ϵ_P varies nonmonotonically with surface temperature, with an overall slight increase with warming occurring in the Lin-graupel simulations and a slight decrease in the Thompson simulations (Figure S4).

In order to understand the deviations of instantaneous precipitation extremes from CC scaling, we need to understand the causes of variations in ϵ_P with temperature. One factor influencing the value of ϵ_P is the fall speed of hydrometeors. A low fall speed results in a longer time between condensation and precipitation, and it increases the probability that a given hydrometeor might evaporate before it reaches the surface (Figure 4a). Additionally, an increased hydrometeor lifetime allows more time for the precipitation event to be smeared out spatially relative to the condensation event by turbulence or the cloud-scale circulation (Figure 4b). While simple advection of the column does not affect ϵ_P (since precipitation extremes and condensation extremes need not be collocated), a horizontal smearing of precipitation over a larger area may contribute to a reduction in ϵ_P. Finally, a low hydrometeor fall speed may also affect ϵ_P by smearing out the precipitation in time. Since condensation occurs at a range of heights, precipitation will reach the ground at different times, even if the condensation were to occur at a single instant. This reduces the magnitude of the maximum instantaneous precipitation rate relative to the maximum column condensation rate, even if it does not alter the total precipitation from a given convective event (Figure 4c). The effect of this temporal smearing on precipitation extremes is thus largest for instantaneous precipitation extremes, while precipitation extremes accumulated over time periods longer than a convective event ($\sim$ 1 hour) may be relatively unaffected.

The hydrometeor fall speed is sensitive to temperature changes; frozen hydrometeors can have significantly different fall speeds compared to that of rain [see, e.g., *Pruppacher and Klett*, 1997]. To investigate the effect that these fall speed changes may have on the response of precipitation extremes to warming, we examine additional intermediate-resolution simulations in which the Lin-hail microphysics scheme is altered such that the fall speeds of all hydrometeors are fixed to a constant value. Sets of simulations are conducted with fall speeds in the range 1–8 m s^{-1}; for each fall speed, simulations are run with different SST boundary conditions corresponding to a subset of the SSTs used in the simulations described in section 2. Apart from the values of the fall speeds of snow, rain, and hail, the model used for each of these simulations is identical to the model used for the corresponding Lin-hail simulation at the same SST (see also section S1). We focus here on the Lin-hail simulations because they exhibit the largest variations in ϵ_P, but changes in fall speeds in the other schemes are also discussed later.
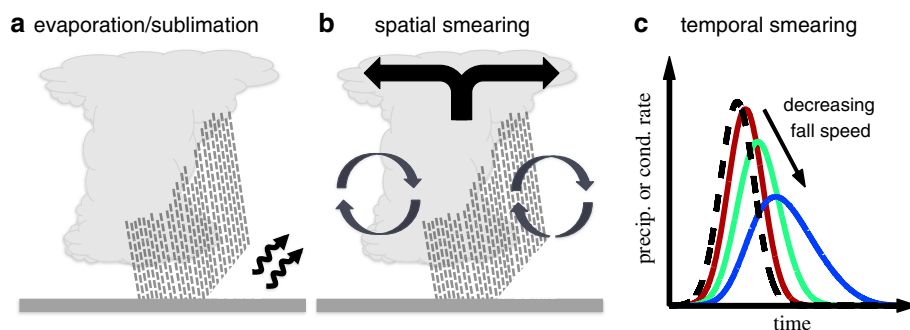
Figure 4. Schematic showing mechanisms affecting the value of the precipitation efficiency, ϵ_P. (a) Evaporation and sublimation of precipitation, (b) spatial smearing of precipitation via removal of liquid and solid water from the column by turbulence (both resolved and subgrid) and the cloud-scale circulation, and (c) smearing of the precipitation event in time as the hydrometeor fall speed decreases (maroon to green to blue). Dashed black line in Figure 4c represents the column net-condensation rate.

Changes in hydrometeor fall speed have a large effect on precipitation extremes (Figure 3b). For example, an increase in fall speed from 1 to 8 m s^{-1} results in an increase in instantaneous precipitation extremes by more than a factor of 5 at a surface temperature of $T_s = 298$ K. That fall speeds influence precipitation statistics is consistent with the results of *Parodi et al.* [2011]. *Parodi and Emanuel* [2009] argue that hydrometeor fall speed also influences updraft velocities because a lower fall speed results in the lofting of a greater quantity of condensed water that then reduces updraft buoyancy through water loading. But in our simulations, net-condensation extremes (Figure 3a), as well as the vertical velocity conditioned on net-condensation extremes (not shown), only weakly depend on fall speed. A stronger dependence of the updraft strength on hydrometeor fall speed is found if only warm-rain microphysical processes are allowed as in *Parodi and Emanuel* [2009], but in general, the effect of fall speed on ϵ_P is a much larger factor in determining the intensity of precipitation extremes.

To quantify the variations in fall speed more generally, we define the effective hydrometeor fall speed, v_f, as the hydrometeor-mass-weighted mean of the fall speeds of all hydrometeors in the column conditioned on the precipitation rate exceeding its 99.99th percentile. In the fixed-fall speed simulations, this is simply equal to the imposed hydrometeor fall speed. In the simulations with the Lin-hail microphysics scheme, v_f ranges from less than 1 m s^{-1} in the coldest simulation to more than 8 m s^{-1} in the warmest simulation (Figure 1b). This is primarily a result of the increasing fraction of rain compared to snow in the column as the atmosphere warms, but the increase in rain mixing ratios with warming also increases the effective fall speed of rain itself (Figures S5a and S5d). Hail has a greater fall speed than both snow and rain, but in the Lin-hail simulations, it contributes only a small fraction of the total hydrometeor loading of the atmosphere.

Based on v_f, and by comparison with the fixed-fall speed simulations, the increase in precipitation extremes with warming in the Lin-hail simulations may be seen to consist of a component related to the increase in surface temperature at fixed fall speed and a component due to the effect of increasing fall speed. The precipitation extremes in a given Lin-hail simulation are roughly consistent with those in a fixed-fall speed simulation at the same surface temperature and with the same effective fall speed (compare marker colors and line colors in Figure 3b), confirming the utility of considering the effects of increasing hydrometeor fall speed separately to other effects of warming.

At fixed fall speed, the increase of precipitation extremes with warming is somewhat below the CC rate and somewhat smaller than the increase in condensation extremes, implying a decrease in ϵ_P with warming (Figure 3b). Part of this reduction in ϵ_P may relate to an increase in hydrometeor lifetime caused by an increase in the mean height over which precipitation falls, since the typical formation height of hydrometeors rises with warming. In the Lin-hail simulations, the increase in effective fall speed v_f amplifies the increase in precipitation extremes with warming. This results in super-CC scaling of instantaneous precipitation extremes at low temperatures (for which the fractional rate of increase in v_f with warming is largest), and it results in roughly CC scaling at temperatures greater than ~ 295 K (for which the hydrometeor distribution is dominated by rain, and the fractional increase in v_f with temperature is smaller).

In simulations using the Lin-graupel and Thompson microphysics schemes, the fractional increase in v_f with warming is smaller than in the Lin-hail case (Figure 1b), and the fractional rates of increase of instantaneous precipitation extremes are also smaller (Figure 1a). The difference in behavior of the fall speed may be attributed to the larger abundance of rimed ice (i.e., graupel or hail) during heavy precipitation events in simulations using these alternate microphysics schemes, which, because of its faster fall speed compared to that of snow, increases the mean hydrometeor fall speed at low temperatures (Figure S5). The smaller increase in v_f with warming in the Lin-graupel and Thompson simulations at least partially accounts for the lower fractional rate of increase of precipitation extremes found with these schemes when compared to the Lin-hail simulations. Other aspects of the microphysical schemes used and the different scaling of condensation extremes in the Thompson simulations may also be expected to contribute to the disagreement of instantaneous precipitation extremes across the different microphysics schemes.

6. Conclusions

Our results show that precipitation extremes in radiative-convective equilibrium increase with warming at a rate roughly consistent with Clausius-Clapeyron scaling at surface temperatures above 295 K. At lower temperatures, uncertainty regarding the representation of ice- and mixed-phase microphysics has a large effect on simulated precipitation extremes, and a variety of behaviors occur.

The fall speed of hydrometeors is found to be one factor influencing the intensity of precipitation extremes. The precipitation rate increases as the hydrometer fall speed is increased because of changes in the efficiency with which large net-condensation events are translated into large precipitation events. The mean hydrometeor fall speed in the simulations increases with warming as the fraction of hydrometeors in the column consisting of frozen species decreases. This amplifies the increase of precipitation extremes relative to the case in which hydrometeor fall speeds are held fixed, particularly for low temperatures at which the fractional change in fall speed with warming is largest.

However, the size of the increase in hydrometeor fall speed is sensitive to the fraction of frozen precipitation existing as rimed ice as well as the fall speed of the rimed ice species itself. Differences in the treatment of frozen hydrometeors at least partially explain the different responses of precipitation extremes to warming in simulations with different microphysics schemes. Indeed, the fall speed characteristics of rimed ice have been found previously to be important in determining the precipitation and radar reflectivities in modeling case studies of supercell [*Morrison and Milbrandt*, 2011] and squall line [*Bryan and Morrison*, 2012] convection.

Other mechanisms not considered in this paper, such as those relating to the formation of precipitating hydrometeors, may also be important for the scaling of precipitation extremes. The scaling of accumulated precipitation extremes does not appear to be related to hydrometeor fall speeds in a simple way, and other dynamical and microphysical factors may play a role in giving the varied behavior of accumulated precipitation extremes found here. Thus, while hydrometeor fall speeds are clearly important in determining the intensity of convective precipitation extremes for short accumulation periods, further work is required to fully understand the mechanisms by which microphysical processes may influence the precipitation distribution in RCE.

Our results may have implications for the behavior of precipitation extremes under climate change or in observed variability in the current climate. For instance, a change in hydrometeor fall speed is one factor that potentially contributes to the super-CC scaling of subdaily precipitation extremes found in some high temporal resolution station observations when stratified by surface temperature [e.g., *Lenderink and van Meijgaard*, 2008; *Lenderink et al.*, 2011; *Berg et al.*, 2013]. Dynamical effects have also been argued to be relevant in explaining the potential for super-CC scaling of precipitation extremes with warming [*Loriaux et al.*, 2013], and relationships between temperature and specific dynamical regimes or moisture availability [*Hardwick Jones et al.*, 2010] complicate the interpretation of precipitation and temperature covariability in observations. This study highlights the role of cloud and precipitation microphysics in helping to determine the response of convective precipitation extremes to warming, and it emphasizes the need for continued research to better constrain the modeling of ice- and mixed-phase precipitation processes.

References

Allan, R. P., B. J. Soden, V. O. John, W. Ingram, and P. Good (2010), Current changes in tropical precipitation, *Environ. Res. Lett.*, *5*, 025205, doi:10.1088/1748-9326/5/2/025205.

Berg, P., C. Moseley, and J. O. Haerter (2013), Strong increase in convective precipitation in response to higher temperatures, *Nat. Geosci.*, *6*, 181–185.

Braun, S. A., and W.-K. Tao (2000), Sensitivity of high-resolution simulations of hurricane Bob (1991) to planetary boundary layer parameterizations, *Mon. Weather Rev.*, *128*, 3941–3961.

Bryan, G. H., and J. M. Fritsch (2002), A benchmark simulation for moist nonhydrostatic numerical models, *Mon. Weather Rev.*, *130*, 2917–2928.

Bryan, G. H., and H. Morrison (2012), Sensitivity of a simulated squall line to horizontal resolution and parameterization of microphysics, *Mon. Weather Rev.*, *140*, 202–225.

Hardwick Jones, R., S. Westra, and A. Sharma (2010), Observed relationships between extreme sub-daily precipitation, surface temperature, and relative humidity, *Geophys. Res. Lett.*, *37*, L22805, doi:10.1029/2010GL045081.

Kendon, E. J., N. M. Roberts, H. J. Fowler, M. J. Roberts, S. C. Chan, and C. A. Senior (2014), Heavier summer downpours with climate change revealed by weather forecast resolution model, *Nat. Clim. Change*, *4*, 570–576.

Kharin, V. V., F. W. Zwiers, X. Zhang, and G. C. Hegerl (2007), Changes in temperature and precipitation extremes in the IPCC ensemble of global coupled model simulations, *J. Clim.*, *20*, 1419–1444.

Lenderink, G., and E. van Meijgaard (2008), Increase in hourly precipitation extremes beyond expectations from temperature changes, *Nat. Geosci.*, *1*, 511–514.

Lenderink, G., H. Y. Mok, T. C. Lee, and G. J. van Oldenborgh (2011), Scaling and trends of hourly precipitation extremes in two different climate zones—Hong Kong and the Netherlands, *Hydrol. Earth Syst. Sci.*, *15*, 3033–3041.

Lin, Y.-L., R. D. Farley, and H. D. Orville (1983), Bulk parameterization of the snow field in a cloud model, *J. Clim. Appl. Meteorol.*, *22*, 1065–1092.

Loriaux, J. M., G. Lenderink, S. R. De Roode, and A. P. Siebesma (2013), Understanding convective extreme precipitation scaling using observations and an entraining plume model, *J. Atmos. Sci.*, *70*, 3641–3655.

Morrison, H., and J. Milbrandt (2011), Comparison of two-moment bulk microphysics schemes in idealized supercell thunderstorm simulations, *Mon. Weather Rev.*, *139*, 1103–1130.

Muller, C. (2013), Impact of convective organization on the response of tropical precipitation extremes to warming, *J. Clim.*, *26*, 5028–5043.

Muller, C. J., P. A. O'Gorman, and L. E. Back (2011), Intensification of precipitation extremes with warming in a cloud-resolving model, *J. Clim.*, *24*, 2784–2800.

O'Gorman, P. A. (2012), Sensitivity of tropical precipitation extremes to climate change, *Nat. Geosci.*, *5*, 697–700.

O'Gorman, P. A., and T. Schneider (2009), The physical basis for increases in precipitation extremes in simulations of 21st-century climate change, *Proc. Natl. Acad. Sci.*, *106*, 14,773–14,777.

Parodi, A., and K. Emanuel (2009), A theory for buoyancy and velocity scales in deep moist convection, *J. Atmos. Sci.*, *66*, 3449–3463.

Parodi, A., E. Foufoula-Georgiou, and K. Emanuel (2011), Signature of microphysics on spatial rainfall statistics, *J. Geophys. Res.*, *116*, D14119, doi:10.1029/2010JD015124.

Pruppacher, H. R., and J. D. Klett (1997), *Microphysics of Clouds and Precipitation*, 2nd ed., 954 pp., Kluwer Acad., Dordrecht, Netherlands.

Romps, D. M. (2011), Response of tropical precipitation to global warming, *J. Atmos. Sci.*, *68*, 123–138.

Singh, M. S., and P. A. O'Gorman (2013), Influence of entrainment on the thermal stratification in simulations of radiative-convective equilibrium, *Geophys. Res. Lett.*, *40*, 4398–4403, doi:10.1002/grl.50796.

Thompson, G., P. R. Field, R. M. Rasmussen, and W. D. Hall (2008), Explicit forecasts of winter precipitation using an improved bulk microphysics scheme. Part II: Implementation of a new snow parameterization, *Mon. Weather Rev.*, *136*, 5095–5115.

Westra, S., L. V. Alexander, and F. W. Zwiers (2013), Global increasing trends in annual maximum daily precipitation, *J. Clim.*, *26*, 3904–3918.

Wicker, L. J., and W. C. Skamarock (2002), Time-splitting methods for elastic models using forward time schemes, *Mon. Weather Rev.*, *130*, 2088–2097.

Wilcox, E. M., and L. J. Donner (2007), The frequency of extreme rain events in satellite rain-rate estimates and an atmospheric general circulation model, *J. Clim.*, *20*, 53–69.